Mechanisms Involved in the Amplification of the 11-yr Solar Cycle Signal in the Tropical Pacific Ocean

STERGIOS MISIOS

Max Planck Institute for Meteorology, and International Max Planck Research School on Earth System Modelling, Hamburg, Germany

HAUKE SCHMIDT

Max Planck Institute for Meteorology, Hamburg, Germany

(Manuscript received 16 May 2011, in final form 1 March 2012)

ABSTRACT

It is debated whether the response of the tropical Pacific Ocean to the 11-yr solar cycle forcing resembles a La Niña– or El Niño–like signal. To address this issue, ensemble simulations employing an atmospheric general circulation model with and without ocean coupling are conducted. The coupled simulations show no evidence for a La Niña–like cooling in solar maxima. Instead, the tropical sea surface temperature rises almost in phase with the 11-yr solar cycle. A basinwide warming of about 0.1 K is simulated in the tropical Pacific, whereas the warming in the tropical Indian and Atlantic Oceans is weaker. In the western Pacific, the region of deep convection shifts to the east, thus reducing the surface easterlies. This shift is independent of the ocean coupling because deep convection moves to the east in the uncoupled simulations too. The reduced surface easterlies cool the subsurface but warm the surface due to the reduction of heat transport divergence. The latter mechanism operates together with water vapor feedback, resulting in a stronger tropical Pacific warming relative to the warming over the tropical Indian and Atlantic Oceans. These results suggest that the atmospheric response to the 11-yr solar cycle drives the tropical Pacific response, which is amplified by atmosphere–ocean feedbacks operating on decadal time scales. Based on the coupled simulations, it is concluded that the tropical Pacific Ocean should warm when the sun is more active.

1. Introduction

The possible influence of the 11-yr solar cycle on the tropical Pacific Ocean has received considerable attention in recent years (e.g., Gray et al. 2010). Yet, it remains under debate mainly due to the shortness of reliable observations of sea surface temperatures (SSTs), which cover only a few solar cycles (Deser et al. 2010). Besides this, modes of natural variability, such as the El Niño–Southern Oscillation (ENSO), and external forcings, such as volcanic eruptions, may veil solar signals in this region. Experiments with coupled atmosphere–ocean general circulation models (AOGCMs), however, could bypass the aforementioned shortcomings because the climatic effect of each forcing can separately be quantified. In this study, we conduct tailored simulations with an AOGCM to investigate whether and how the tropical oceans, particularly the Pacific Ocean, respond to the 11-yr solar cycle forcing.

Past analyses demonstrated either an anomalously cold or warm tropical Pacific with increased solar activity. Filtering of bathythermograph data from 1955 to 1994 identified positive SST anomalies with El Niño–like spatial characteristics, oscillating almost in phase with the 11-yr solar cycle (White et al. 1997). Multiple linear regression analysis of the boreal winter SSTs over the second half of the twentieth century indicated a somewhat comparable band of warm water along the equatorial Pacific in solar maxima (Roy and Haigh 2010). Curiously, the increased solar activity was related to negative SST anomalies in the eastern Pacific when longer datasets (e.g., 1880–2008) were analyzed (Roy and Haigh 2010; Tung and Zhou 2010). The El Niño–like warming was initially attributed to direct solar heating (White et al. 1997) but later it was related to the solar

Corresponding author address: Stergios Misios, Max Planck Institute for Meteorology, Bundesstrasse 53, 20146 Hamburg, Germany.
E-mail: stergios.misios@zmaw.de

DOI: 10.1175/JCLI-D-11-00261.1

cycle excitation of the tropical Pacific quasi-decadal oscillation (TPQDO) (White and Liu 2008b). The TPQDO, however, is an atmosphere–ocean mode of the tropical Pacific, excited naturally in many AOGCMs even with constant solar forcing (Cibot et al. 2005; Knutson and Manabe 1998).

In contrast, the composite analysis of van Loon et al. (2007) detected a La Niña–like cooling in peak years of sunspot numbers (SSNs). To explain such a response, Meehl et al. (2008) suggested that direct heating of the ocean surface due to increased total solar irradiance (TSI) in solar maxima releases more water vapor that converges into precipitation zones, fueling the meridional (Hadley) and zonal (Walker) overturning circulations with extra energy. When the Walker circulation speeds up, the surface temperature decreases because more cold water is upwelled in the eastern Pacific. Amplified subsidence and negative SST anomalies in this region should further reduce the cloud coverage, allowing stronger radiative heating. This positive feedback, commonly termed the ''bottom-up'' mechanism (Gray et al. 2010), could shift the tropical Pacific system to a La Niña–like state. A weak cooling in the tropical Pacific in peak years of SSNs was simulated employing AOGCMs with poor representation of stratospheric dynamics (Meehl et al. 2003, 2008). The inclusion of stratospheric dynamics amplified the cooling in a simulation by Meehl et al. (2009). This led to the proposition that the stratospheric response to enhanced ultraviolet radiation and ozone (''top-down mechanism'') may act together with the bottom-up mechanism to amplify solar-cycle signals in the tropical Pacific (van Loon et al. 2007; Meehl et al. 2009). The modeling study of Bal et al. (2011) also indicated a La Niña–like cooling in solar maxima.

The suggestion for a La Niña–like cooling was based on boreal winter [December–February (DJF)] SST anomalies (relative to climatology) in peak years of SSNs (SSN_MAX). The response of the tropical Pacific in years of minimum SSNs (SSN_MIN) was not studied. According to the bottom-up mechanism, less moisture should be transported to the convergence zones in SSN_MIN, resulting in a weaker Walker circulation. Consequently, the tropical Pacific should shift from negative SST anomalies in SSN_MAX to positive anomalies in SSN_MIN. Yet, observations do not substantiate such a transition. The Extended Reconstruction SST version 3b (ERSSTv3b) (Smith et al. 2008), for instance, indicates negative temperature anomalies in composites of both SSN_MAX and SSN_MIN (Fig. 1). This raises questions about the validity of the proposed mechanism and subsequently about the origin of the putative solar cycle signals.

The La Niña–like cooling in SSN_MAX could reflect an accidental oversampling of La Niña events instead of a genuine solar cycle signal. Tung and Zhou (2010) highlighted that 9 of the 12 years used in the SSN_MAX composite belong to cold ENSO, whereas the distribution of cold/warm ENSO episodes in SSN_MIN is more even. This fact could explain the well-formed La Niña signature in SSN_MAX and subsequently the absence of a strong response in SSN_MIN (Fig. 1). Yet, it cannot be excluded that the increased solar forcing favors, statistically, a La Niña excitation. This notion was supported by White and Liu (2008a), who suggested a nonlinear mechanism by which the solar cycle excites La Niña and El Niño pairs during its rising phase. In this context, the El Niño–like warming was interpreted as a delayed, wave-driven reaction to earlier cooling in peak years of solar activity (Meehl and Arblaster 2009).

Observational evidence for a cold eastern Pacific in solar maxima has been provided by a number of independent studies employing elaborate statistical methods (Camp and Tung 2007; Tung and Camp 2008; Tung and Zhou 2010; Zhou and Tung 2010). The detected spatial patterns, however, resembled neither La Niña– nor El Niño–like conditions. Instead, these studies documented a weak zonal SST dipole with positive (negative) anomalies in the western (eastern) sector of the tropical Pacific. The ocean dynamical thermostat mechanism (Clement et al. 1996) could explain this dipole, provided that the tropical Pacific basin is heated uniformly during solar maxima.

To summarize, previous observational and modeling analyses agree neither on the sign nor on the spatial pattern of the Pacific response to the 11-yr solar cycle. In this study, we question whether the tropical Pacific Ocean shifts to a La Niña–like state in solar maxima. To give an answer and to identify physical mechanisms, we carry out ensemble simulations with an AOGCM. In section 2, we describe the model, the experimental setup, and the analysis procedures. In section 3, the simulated interannual and decadal variability of the tropical Pacific is assessed. Next, the response of the tropical atmosphere–ocean system to the 11-yr solar cycle is isolated in ensemble simulations with ocean coupling, whereas solar signals in atmosphere-alone simulations are presented in section 6. Possible shortcomings of our model are listed in section 7, and the findings of this study are summarized and discussed in section 8.

2. Data and methods

a. Model description and experimental design

We performed ensemble simulations with the middle atmosphere version of the ECHAM5 (MAECHAM5)

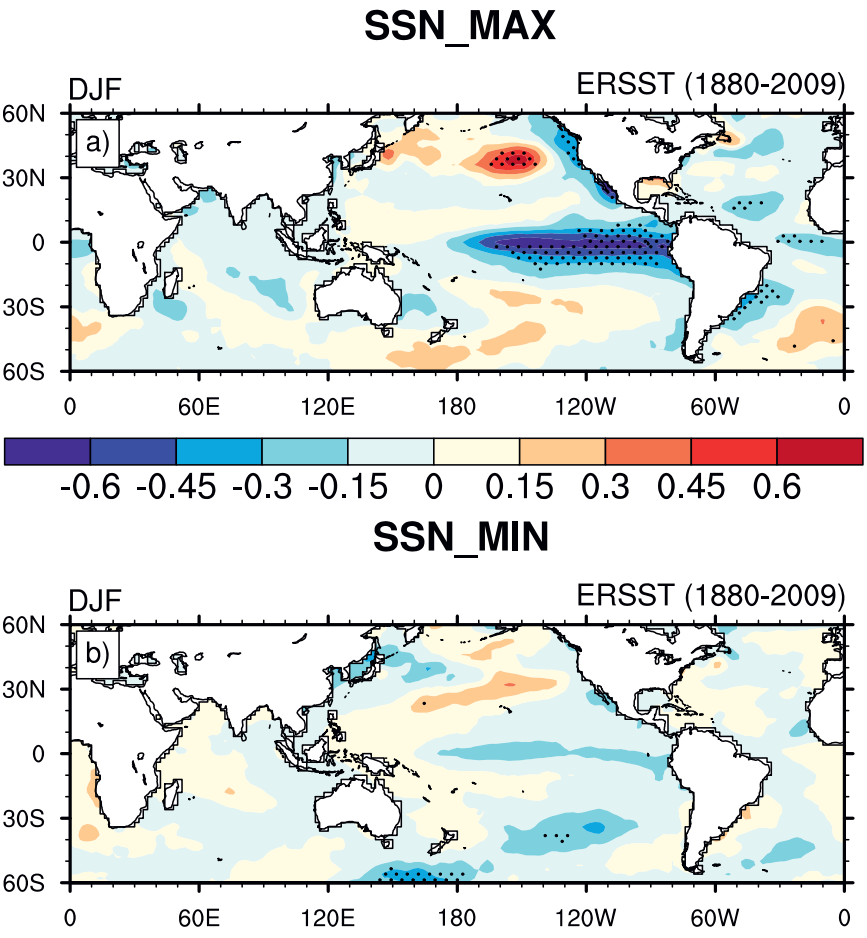

FIG. 1. DJF-averaged SST anomalies (K) from the ERSSTv3b reconstruction (1880–2009) for (a) years of peak maximum sunspot numbers (1883, 1893, 1905, 1917, 1928, 1937, 1947, 1957, 1968, 1979, 1989, 2000) and (b) years of peak minimum susnspot numbers (1889, 1901, 1913, 1923, 1933, 1944, 1954, 1964, 1976, 1986, 1996, 2008). Anomalies are calculated with respect to the 1880–2009 climatology. To eliminate the nonlinear positive trend (Thompson et al. 2008), a high-pass filter (subtraction of 156-month running average) was applied prior to compositing. Stippling indicates 95% significance according to a bootstrap test of 10 000 surrogates. Figure 1a after van Loon et al. (2007).

general circulation model (Manzini et al. 2006; Roeckner et al. 2006) coupled to the Max Planck Institute Ocean Model (MPI-OM) (Marsland et al. 2003). The Ocean–Atmosphere–Sea Ice–Soil (OASIS) coupler without any flux correction is responsible for momentum, heat, and freshwater exchanges between atmosphere and ocean (Valcke et al. 2003). The CO_2 concentration is fixed at 348 ppm. The atmospheric resolution is T31L90, denoting spectral truncation at wavenumber 31 (equivalent to a 3.75° × 3.75° grid) and 90 vertical levels (up to 0.01 hPa), whereas the ocean curvilinear grid has 3° resolution at the equator and 40 vertical levels. We have chosen this fairly coarse resolution to allow for a large number of ensemble runs. Compared to earlier modeling attempts (e.g., Meehl et al. 2008; Rind et al. 2008; Meehl et al. 2009), it is the first time when a fully AOGCM with spontaneously generated stratospheric quasi-biennial oscillation is employed to study effects of solar variability.

With respect to the model version described by Manzini et al. (2006), several modifications were introduced to MAECHAM5 so as to simulate a realistic and transient 11-yr solar cycle. More specifically, we prescribe spectral solar irradiance changes that conform to the recommendations of the Chemistry–Climate Model Validation (CCMVal) activity (Eyring et al. 2010). The shortwave radiation parameterization of MAECHAM5 accommodates six spectral bands, resulting in improved representation of ozone absorption compared to older versions (Cagnazzo et al. 2007).

Because MAECHAM5 is not coupled to a chemistry scheme to account for ozone photochemistry, the effects of solar cycle variability on ozone need to be parameterized. For this reason, we add to the background ozone climatology the annual cycle of the solar-cycle-induced ozone anomalies taken from the Hamburg Model of the Neutral and Ionized Atmosphere (HAMMONIA) simulations in perpetual solar maximum/minimum conditions (Schmidt et al. 2010). The prescribed ozone anomalies are scaled with the daily 10.7-cm solar radio flux (F10.7) to introduce an 11-yr variation. It must be noted that radiative forcing from 1) the increasing greenhouse gas concentrations and 2) the aerosol loading from volcanic eruptions is deliberately excluded to ease interpretation.

An ensemble of 11 realizations with realistic solar spectral variations from 1955 to 2006 is carried out (CENS). Each run branches from a different initial condition, taken from a 140-yr unperturbed control run (CTR). A separate ensemble of nine realizations of MAECHAM5 without ocean coupling is additionally carried out (AENS). The model setup is the same as in CENS except that AENS is forced with SST and sea ice fraction climatologies from CTR. The analysis of AENS will demonstrate the atmospheric response to solar forcing, neglecting atmosphere–ocean feedbacks.

b. Analysis procedures

Unless stated otherwise, our analysis of the solar-cycle-forced simulations deals with ensemble-mean annual time series after the annual cycle has been removed. To extract solar cycle signals, anomalies of various meteorological variables are regressed onto the annual F10.7 flux. We additionally use lagged versions of the variables in the regression model to illustrate the time evolution of the solar cycle responses. All regression coefficients are scaled per 100 units of F10.7 (100 sfu) to ease comparison with previous studies. The response of a ''typical'' solar cycle can be derived by multiplying with ~1.3. The statistical significance is examined with a standard two-tailed t test after the $n - 2$ sample size ($n - 2 = 50$) is corrected to account for the effect of autocorrelation of the dependent variable [Eq. (5.12) in Wilks 2006].

The natural variability of the tropical oceans on decadal time scale needs to first be assessed before effects of the 11-yr solar cycle are examined. This is because MAECHAM5/MPI-OM generates internally a well-pronounced decadal variability, which is isolated with the multichannel singular spectrum analysis (MSSA) toolbox (Ghil et al. 2002). A 10-channel MSSA with a 17-yr window length calculates the time EOFs (T-EOFs) and the corresponding time principal components (T-PCs) of the tropical (30°S–30°N) annual SST anomalies in CTR. The observed evidence for a decadal SST variability of a 9–12-yr period (TPQDO) dictated the chosen window length (White et al. 2003). The first six T-EOFs describe ENSO and other intradecadal frequencies, whereas the time evolution of the seventh and eighth T-EOFs (each T-EOF explains 4% of the interannual SST variability) exhibits well-pronounced spectral peaks at 12.5 yr. Moreover, the seventh and eighth T-EOF–T-PC pair show a phase–quadrature relationship that characterizes oscillatory modes (Plaut and Vautard 1994). This pair captures the naturally excited decadal variability of the tropical Pacific (TPQDO) and is used to reconstruct the associated SST anomalies. Finally, the spatial signature of the simulated TPQDO in CTR is obtained by regressing the TPQDO index (the normalized first PC of the MSSA-reconstructed annual SST anomalies) onto the raw SST anomalies [units in kelvin per one standard deviation of the TPQDO index (K std^{-1})].

In section 4, MSSA is complementary used to filter ensemble-mean annual SST anomalies from CENS. One advantage of the MSSA over linear regression is that no a priori information about the external forcing is required (e.g., the 11-yr solar cycle). The analysis is limited within the tropical latitudes because significant solar signals are detected only over this region. A 10-channel MSSA with 14-yr window length calculates T-EOF–T-PC pairs. Similar to CTR, the first six pairs describe ENSO and other intradecadal frequencies, whereas the spectrum of the seventh and eighth T-PCs (explaining 4.2% and 4.1% of the total interannual SST variability) peaks at 10.9 yr. This period approximates the average solar cycle period from 1955 to 2006 (10.4 yr). MSSA-filtered annual SST anomalies (MSSA-SST) are then reconstructed by considering only the seventh and eighth T-EOF–T-PC pairs. In essence, the MSSA acts as a bandpass filter of a narrow frequency range.

3. Interannual and decadal tropical Pacific SST variability in the control simulation

The coupled ECHAM5/MPI-OM with a lower lid (10 hPa) has been previously employed in numerous studies, including the Coupled Model Intercomparison Project phase 3 (CMIP3) simulations (e.g., Jungclaus et al. 2006). Because it is the first time that results from MAECHAM5/MPI-OM are documented, we briefly evaluate the simulated mean state, interannual, and decadal variability of the tropical Pacific Ocean, the main region of interest throughout this paper.

Similar to the majority of the AOGCMs of this class (e.g., Reichler and Kim 2008), our model shows a cold bias in the climatological state of the equatorial eastern Pacific. The comparison of the SST climatology in CTR

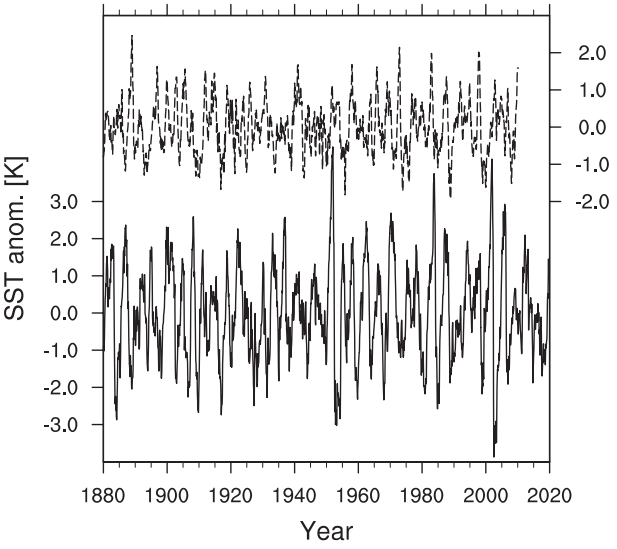

FIG. 2. Time series of the monthly Niño-3.4 index (K) from the ERSSTv3b reconstruction over the period 1880–2009 (dashed line). A high-pass filter has been applied (subtraction of 156-month running average). Time series of the simulated monthly Niño-3.4 index in CTR (solid line). Time indexing is valid for observations only.

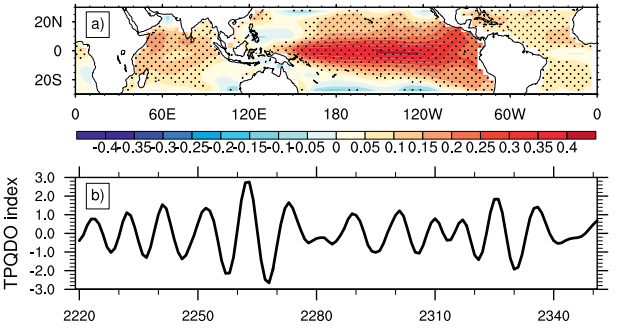

FIG. 3. (a) Regression coefficients (K std^{-1}) of the unfiltered annual SST anomalies in CTR onto the TPQDO index (see section 2b for the definition of the TPQDO index). Stippling indicates 95% significance. (b) Time series of the TPQDO index in CTR.

versus the ERSST climatology (1880–2009) shows essentially the same pattern as in Fig. 3a in Jungclaus et al. (2006), so it is not shown here. The inclusion of the middle atmosphere does not alter significantly the precipitation patterns along the tropical Pacific. Double intertropical convergence zones (ITCZs) are simulated, a common flaw of many AOGCMs (Guilyardi et al. 2003).

To diagnose the interannual variability of the tropical Pacific, we evaluate the monthly Niño-3.4 index (SST anomalies over the region 5°S–5°N, 120°–170°W) in CTR. Figure 2 emphasizes that the simulated ENSO is more cyclic compared to the observed one, given that strong La Niña episodes follow most strong El Niño episodes. Additionally, the simulated ENSO amplitude is much stronger (standard deviation of 1.28 K in CTR versus 0.7 K in ERSSTv3b), which complicates, as we see later, the detection of solar signals in the tropical Pacific. Nevertheless, the average period of the simulated ENSO (3.6 yr) lies within the observed range from 3 to 7 yr.

Akin to many AOGCMs (Cibot et al. 2005; Knutson and Manabe 1998), MAECHAM5/MPI-OM generates internally a TPQDO with an average period of 12.5 yr. The spatial signature of the simulated TPQDO on SSTs is marked by a basinwide warming up to 0.3 K std^{-1}, flanked by negative anomalies in the extratropics (Fig. 3a). Over the north Indian Ocean and most of the tropical Atlantic Ocean, the positive phase of the TPQDO isassociated with positive but weaker SST anomalies compared to the tropical Pacific. The time evolution of the TPQDO index indicates pronounced multidecadal variations (Fig. 3b). As in observations (e.g., Hasegawa and Hanawa 2003), the simulated TPQDO is explained by the recharge/discharge mechanism of ENSO (Jin 1997) operating, however, on decadal time scales. A separate analysis, not presented here, identifies positive ocean heat content anomalies (averaged over the equatorial Pacific) that lead positive Niño-3.4 anomalies by about two years. A similar phase relationship has been observed during El Niño events (Meinen and McPhaden 2000). From this point of view, the TPQDO can be perceived as an extension of the ''classic'' ENSO to lower frequencies (Tourre et al. 2005).

4. Tropical responses to the solar cycle in the coupled simulations

a. Temporal evolution of tropical SST anomalies

Owing to the unrealistically large ENSO amplitude (section 3), a considerable fraction of the simulated ENSO variability is visible even after averaging over 11 ensemble members. This is evident in Fig. 4a, which shows the time evolution of the ensemble-mean SST anomalies in CENS averaged over the equator (5°S–5°N). In the Pacific positive anomalies up to 0.6 K follow negative anomalies of comparable magnitude and vice versa. It is difficult to identify a solar signal in this plot. Figure 4a highlights the difficulty of detecting solar signals in the equatorial Pacific when short time series are considered because any composite analysis would be prone to ENSO contamination.

ENSO episodes may shade, however, weak solar signals in the tropical Pacific. The MSSA-SST reconstruction shows that, indeed, a weak solar signal is shaded by ENSO because the equatorial Pacific warms (cools) almost in phase with stronger (weaker) solar activity

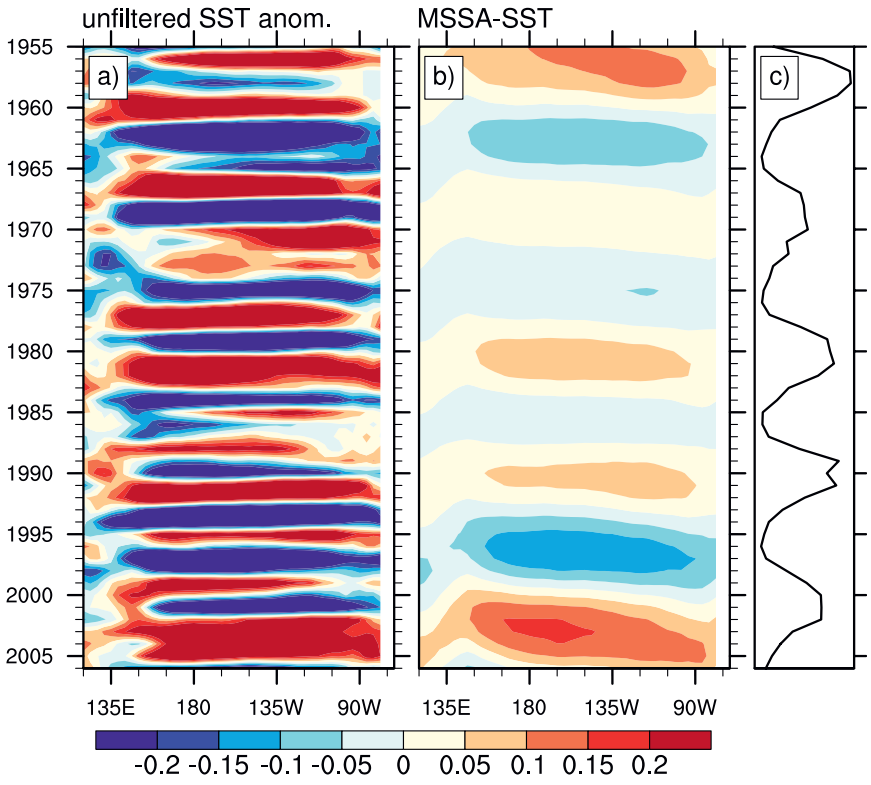

FIG. 4. Hovmöller diagram of the ensemble-mean annual (a) unfiltered and (b) MSSA-filtered anomalies (K) at the equator (5°S–5°N). (c) F10.7 is shown for reference.

(Fig. 4b). The average magnitude of the warming from solar minima to solar maxima (0.13 K) is considerably lower than the ENSO-related variations in the unfiltered time series (1.2 K).

Unambiguous solar cycle signals in particular locations can be detected even in the unfiltered SST time series. For example, the western equatorial Pacific (10°S–10°N, 130°–150°E) warms in phase with the solar cycle. The peak-to-peak amplitude of the 7-yr low-pass-filtered time series (Lanczos filter with nine weights) is approximately 0.1 K. The correlation coefficient between the unfiltered time series and F10.7 is 0.4 (significance >95%). In contrast, poor correlations are calculated over the central and eastern equatorial Pacific due to the strong ENSO influence.

The unfiltered SST anomalies averaged over the tropical oceans consist of high- and low-frequency components (Fig. 5b). The former is related to ENSO while the latter is the solar cycle response, which is isolated with the MSSA. The tropical oceans in MSSA-SST warm (cool) with stronger (weaker) solar activity, with a maximum amplitude of approximately 0.05 K. The low-frequency tropical warming seems to lag the 11-yr solar cycle, given that the correlation coefficient between the tropical average MSSA-SST and F10.7 maximizes at lag +1 year ($r = 0.67$).

The MSSA filtering may introduce spurious lags because it is based on a narrow frequency band (i.e., 10.9-yr), whereas the length of every solar cycle is not constant but varies from 9 to almost 14 years. To assess the validity of the MSSA reconstruction, we filter F10.7 with the singular spectrum analysis (SSA). SSA is the single-channel variation of MSSA (Ghil et al. 2002). The first and second T-PC pair capture an oscillation of 10.4 years that is, as already mentioned, the average period of the solar cycle over 1955–2006. The SSA-filtered F10.7 time series is then reconstructed following a methodology similar to that described in section 2b. On the basis that the SSA-reconstructed F10.7 shows no spurious time lag when compared to unfiltered F10.7, we conclude that the time delay of MSSA-SST, most notable after 1995 (solar cycle 23), is a genuine feature of CENS. This is further supported by the unfiltered time series in Fig. 5b, which shows a similar delay after 1995. White et al. (1998) elaborate on the reasons why signals at the ocean surface may lag the 11-yr solar forcing by 1–2 yr.

The MSSA filtering isolates a quasi-decadal oscillation that aligns with the 11-yr solar cycle (lag +1 correlation: 0.67). Because only five solar cycles are simulated, it is possible that the reconstructed oscillation merely reflects a random alignment to the solar cycle of the otherwise

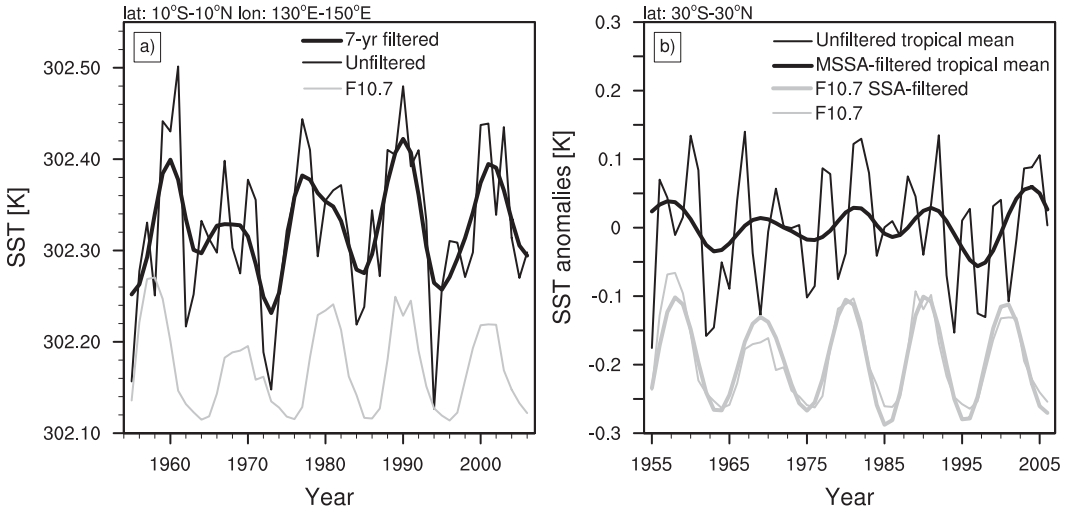

FIG. 5. (a) Time series of the ensemble-mean annual SST anomalies (K) (thin black line) averaged over the western Pacific (10°S–10°N, 130°–150°E). The 7-yr low-pass-filtered (Lanczos filter) time series are shown with the thick black line. (b) Time series of the unfiltered ensemble-mean annual SST anomalies (thin black line) and MSSA-SST (thick black line) averaged over the tropical oceans (30°S–30°N). Unfiltered (thin gray line) and SSA-filtered (thick gray line) annual F10.7 from 1955 to 2006 are superimposed for reference.

naturally excited quasi-decadal variability (TPQDO). To estimate the probability of deriving a lag +1 correlation equal to 0.67 by random processes, we use the CTR simulation in which the TPQDO is certainly not related to the 11-yr solar cycle. Following the method of Zhou and Tung (2010), a set of 10 000 synthetic ensemble-mean TPQDO indices are generated with a block-bootstrap resampling. Every ensemble consists of 11 phantom members, and every member is constructed by selecting randomly the first only year of a 52-yr "chunk" of the TPQDO index (Fig. 3b). Hence, the block size of the bootstrap resampling is 52 years, a conservative estimate.

Figure 6 displays the probability density function of the lag +1 correlation coefficient derived from the random resampling of the TPQDO index in CTR. According to this test, the lag +1 correlation coefficient calculated in the solar-cycle-forced simulations passes the 95% threshold. In other words, there is less than 5% chance that one would obtain a lag +1 correlation higher than 0.67 by superimposing 11 independent, unforced model integrations. This test suggests that the quasiperiodic oscillation in CENS detected with MSSA is not explained by random sampling of the TPQDO but from physical reasons. The physical mechanism, which warms the tropical oceans in solar maxima, is described in the following sections.

b. *Spatial patterns of SST and precipitation*

Figure 7a presents the simultaneous regression coefficients of the SST anomalies from CENS onto F10.7. The response does not change much when the lag +1 regression coefficients are calculated. It must be noted that the tropical Pacific warms rather symmetrically with respect to the equator but significant anomalies (>95%) are detected in the western sector only. Negative anomalies in the extratropics flank positive anomalies in the tropics. Over the north Indian Ocean and most of the tropical Atlantic Ocean, positive SST anomalies are also simulated but with weaker magnitude. Negative anomalies are seen off the Australian west coast. The zonal-mean response peaks at the equator, reaching values of 0.08 K $(100\ \text{sfu})^{-1}$. To verify the robustness of the solar signals in CENS, we present the regression coefficients of the MSSA-SST onto F10.7 (Fig. 7b). The statistical significance is omitted because it exceeds the 95% threshold almost everywhere. Figure 7b is consistent with Fig. 7a but some subtle differences are also identified. The eastern Pacific seems to warm less in the MSSA-SST compared to the unfiltered SSTs. Owing to filtering, the regression coefficients are now slightly weaker in the zonal average.

In many individual ensemble members, the regression analysis isolates a clear La Niña response in solar maxima. However, the ensemble-mean response takes El Niño–like spatial characteristics. This underlines the necessity for large ensembles in order to obtain reliable solar signals. The Pacific warming in Fig. 7 could also be characterized as TPQDO like, but the bootstrap test explained in the previous section gives confidence that this warming is not explained by a random sampling of the TPQDO.

The simulated warming in the tropical Pacific agrees well with the observed solar cycle signals from 1955 to 1994 documented by White et al. (1997). The agreement is quantitative, given that the warming [0.12 K $(100\ \text{sfu})^{-1}$]

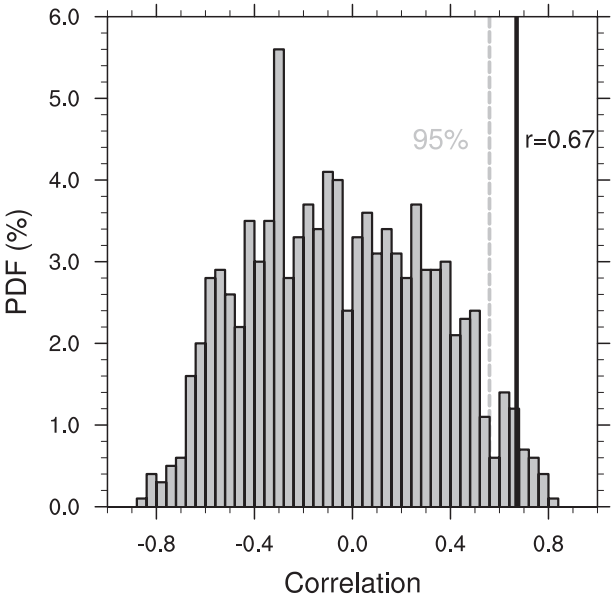

FIG. 6. Probability density function (PDF) of 10 000 synthetic lag +1 correlation coefficients between the ensemble-mean (11 members) TPQDO index and F10.7. Every synthetic ensemble-mean TPQDO index has been generated from the TPQDO index in CTR (Fig. 3b) with block bootstrapping: the block size is set to 52 yr. The dashed gray line indicates the 95% confidence level, and the thick black line indicates the lag +1 correlation between the tropical average MSSA-SST in CENS and F10.7 ($r = 0.67$).

in CENS compares with the observed warming of 0.15 K from solar minimum to solar maximum. Likewise, the tropical Pacific response in Fig. 7a is qualitatively consistent with the solar cycle warming detected by Roy and Haigh (2010), considering SSTs over the second half of the twentieth century. The correspondence is not limited to the tropical Pacific Ocean only but extends to the tropical Indian and Atlantic Oceans as well.

As emphasized in the introduction, the observed solar cycle signature in the tropical Pacific depends substantially on the analysis method and period under investigation. Spatiotemporal filtering of the reconstructed SSTs from 1880 to 2008 isolated a zonal dipole with cooling in the eastern Pacific and warming in the western Pacific (Zhou and Tung 2010). Similarly, spatiotemporal filtering of SSTs over the second half of the twentieth century returned a comparable zonal dipole (Camp and Tung 2007; Tung and Camp 2008), but bandpass temporal filtering detected a basinwide warming (White et al. 1997). Multiple linear regression analysis of SSTs after the 1950s returned a basinwide warming in solar maxima (Roy and Haigh 2010). In contrast, multiple linear regression of longer SST time series (1880–2009) detected a zonal SST dipole (Roy and Haigh 2010; Tung and Zhou 2010). The reason for these discrepancies remains unknown, but it could partly be related to the scarcity of observations in the tropical Pacific before the 1940s (Deser et al. 2010). Moreover, it is possible that the aforementioned statistical analyses may not adequately separate solar cycle signals from ENSO or other decadal variations of the tropical Pacific. Otherwise it is difficult to understand why the effects of the 11-yr solar cycle change between the first and second half of the twentieth century. Our simulations put forward the observation-based notion for anomalous warming in the tropical Pacific in solar maxima.

A warmer sea surface should increase the boundary layer moisture, which in turn may alter the hydrological cycle (Held and Soden 2006). Simulated changes of total precipitation with stronger solar activity are depicted in Fig. 8. Over the western Pacific the total precipitation increases by more than 0.2 mm day^{-1} (100 sfu)$^{-1}$. Although the signal is small and of low significance, its spatial pattern in the Pacific Ocean indicates stronger precipitation in the ITCZ. The zonal-mean solar response is positive at 10°N and slightly negative close to 20° in both hemispheres. The positive–negative dipole between 140° and 170°E implies a northward displacement of the South Pacific convergence zone. These changes are not unique in MAECHAM5/MPI-OM but have been simulated with other coupled models (e.g., Shindell et al. 2006). A separate analysis of the seasonal dependence of precipitation changes identifies the strongest signal in the June–August season, consistent with observations (van Loon et al. 2004). An explanation of the precipitation response is postponed until section 5a.

A number of studies found positive correlations between the sea level pressure (SLP) in the Gulf of Alaska and the 11-yr solar cycle (e.g., Christoforou and Hameed 1997; van Loon and Meehl 2011). The positive SLP anomalies in solar maxima were linked to the La Niña–like cooling in the tropical Pacific, although changes in the stratosphere due to excess UV heating may lead to similar SLP responses (Matthes et al. 2006). In CENS, the Aleutian low in the Gulf of Alaska deepens with stronger solar cycle forcing (not shown), as expected from the simulated El Niño–like warming. Such a SLP response, which opposes previous suggestions, can be explained by a Rossby wave excitation due to convective precipitation and heating changes in the western Pacific.

5. Mechanisms responsible for surface warming

a. Surface heat flux budget

Insight into the physical mechanisms causing the warming in the tropics can be gained by compiling the different components of the heat flux budget at the surface. The downward solar radiation averaged over the

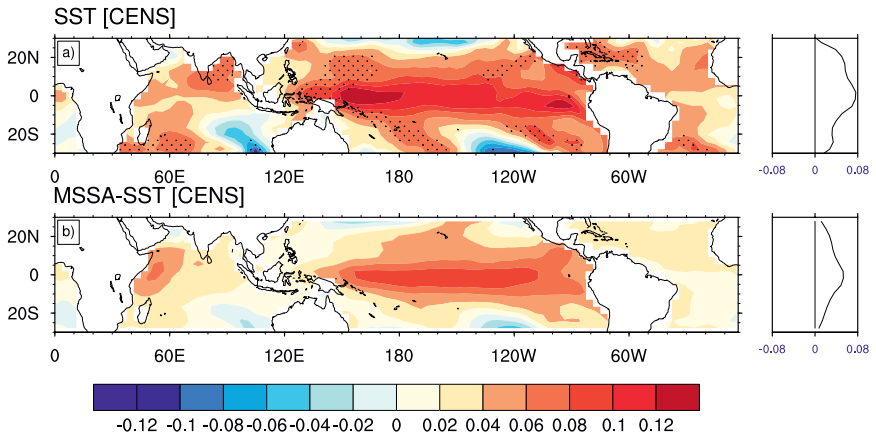

FIG. 7. (left) Regression coefficients onto F10.7 of the ensemble-mean annual (a) SST anomalies and (b) MSSA-SST [K (100 sfu)$^{-1}$]. Stippling in (a) indicates 95% significance. Significance in (b) is omitted because it exceeds the 95% threshold almost everywhere. (right) Zonal averages are plotted.

inner tropics (10°S–10°N) increases by 0.19 W m^{-2} (100 sfu)$^{-1}$ with increasing solar forcing. Locally, much stronger positive or negative anomalies are simulated (Fig. 9e). In the Pacific, for instance, the downward solar radiation increases by 0.53 W m^{-2} (100 sfu)$^{-1}$ in the eastern part, whereas it reduces by 0.3 W m^{-2} (100 sfu)$^{-1}$ in the western part. As shown later, these changes are coming from cloud changes.

The enhanced downward radiation should warm the surface, particularly over the cloud-free regions and in areas where the cloud fraction is reduced (e.g., at the eastern Pacific; see later). Responding to this warming, the oceans should release extra latent heat into the atmosphere. As seen in Fig. 9a, the zonal-mean column-integrated water vapor, a quantity that reflects humidity changes in the boundary layer (Held and Soden 2006), increases by 0.6% (100 sfu)$^{-1}$ compared to the CTR climatology or by 0.6%/0.08 K if the simulated warming is accounted. The latter value follows closely the Clausius–Clapeyron relationship. Moistening of the lowermost troposphere in solar maxima has been also documented in simulations with perpetual maximum/minimum solar forcing (Lee et al. 2009).

The enhanced near-surface water vapor in solar maxima should diminish the clear-sky net shortwave flux (Q_{SW}) and strengthen the net longwave flux (Q_{LW}) at the surface. Indeed, the net clear-sky Q_{SW} over the inner tropics is slightly reduced [−0.02 W m^{-2} (100 sfu)$^{-1}$], opposing the considerable increase of the net clear-sky Q_{LW} [0.3 W m^{-2} (100 sfu)$^{-1}$, see Table 1]. Overall, the moistening of the troposphere results in positive changes of the net clear-sky radiation in the inner-tropical sea surface [0.28 W m^{-2} (100 sfu)$^{-1}$]. Despite that the specified tropospheric ozone increases in solar maxima, its contribution to the longwave absorption is trivial. Hence, the clear-sky radiation budget is influenced mainly by the water vapor changes. For this reason, the spatial patterns of the net clear-sky radiation changes (Fig. 9b) follow closely the water vapor changes (Fig. 9a).

The zonal-mean cloud fraction in the inner tropics reduces with increasing solar forcing (Fig. 9c). However, the response is zonally asymmetric. The cloud fraction increases by 1.6% (100 sfu)$^{-1}$ over the western Pacific while it decreases in the eastern Pacific. The latter reflects a reduction of low stratiform clouds (not shown), which can be explained by the thermodynamic considerations

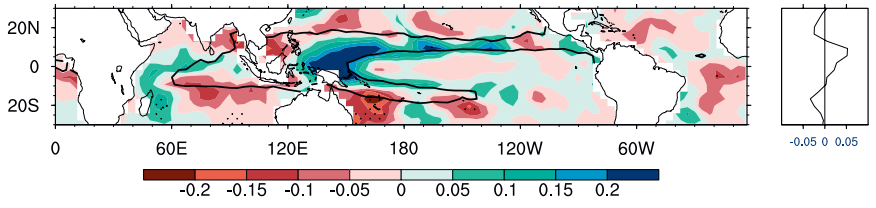

FIG. 8. (left) Regression coefficients onto F10.7 of the ensemble-mean annual total precipitation [mm day^{-1} (100 sfu)$^{-1}$] in SENS. Stippling indicates 95% significance; the thick black line outlines areas where the total precipitation climatology in CTR exceeds 6 mm day^{-1}. (right) Zonal averages are plotted.

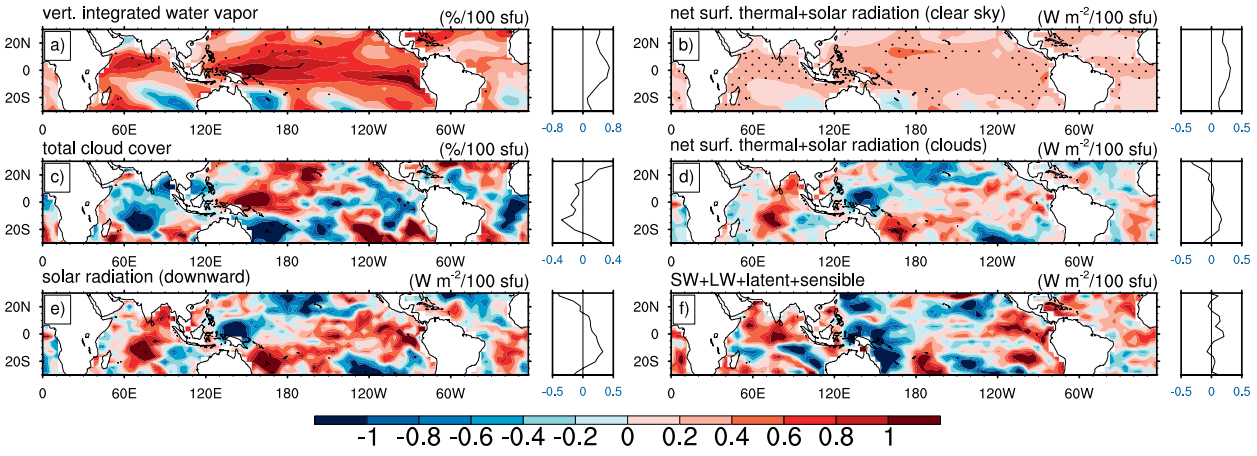

FIG. 9. Regression coefficients onto F10.7 of the ensemble-mean annual anomalies of the (a) vertically integrated water vapor [% (100 sfu)$^{-1}$], (b) clear-sky net surface radiation [W m^{-2} (100 sfu)$^{-1}$], (c) total cloud cover [% (100 sfu)$^{-1}$], (d) net surface radiation due to cloud changes (W m^{-2}), (e) downward solar radiation at the sea surface [W m^{-2} (100 sfu)$^{-1}$], and (f) the sum of net shortwave, longwave, latent, and sensible surface heat fluxes [W m^{-2} (100 sfu)$^{-1}$]. Stippling indicates 95% significance. Zonal averages are plotted to the right. In (b),(d), (e), and (f) positive values point to the ocean.

of Klein and Hartmann (1993), involving changes in static stability. Although this pattern resembles that of a stronger Walker circulation, the deep convection over the Maritime Continent is not getting stronger but, as shown below, it shifts somewhat to the east. Over the equatorial Indian Ocean, the negative cloud fraction anomalies are associated with stronger adiabatic heating due to enhanced descent (not shown).

The zonal-mean change of the net shortwave radiation due to cloud changes, Q_{SW}(cloud), increases by 0.19 W m^{-2} (100 sfu)$^{-1}$ in the inner tropics, whereas the net longwave radiation, Q_{LW}(cloud), decreases by 0.13 W m^{-2} (100 sfu)$^{-1}$. Note that the cloud forcing is calculated by subtracting clear-sky from all-sky Q_{SW} and Q_{LW}, respectively. The spatial patterns of Q_{SW}(cloud) + Q_{LW}(cloud) are depicted in Fig. 9d, in which the positive values point to the ocean. The cloud forcing anomaly averaged over the inner tropics is negligible [0.06 W m^{-2} (100 sfu)$^{-1}$] but spatially inhomogeneous for reasons previously explained. Locally, strong radiative warming/cooling with values up to 1.6 and −1.8 W m^{-2} (100 sfu)$^{-1}$, respectively, is simulated.

Table 1 emphasizes that, in a zonally averaged perspective, the surface heating due to the water vapor feedback is considerably stronger than the forcing due to cloud changes. This stems from the zonal uniformity of the former compared to the spatial heterogeneity of the latter. Locally (e.g., in the central and eastern equatorial Pacific), however, surface heating due to cloud changes outpaces the water vapor feedback. The zonal-mean radiative surface heating is balanced partly by stronger latent heat release [0.27 W m^{-2} (100 sfu)$^{-1}$, see Table 1]. When changes in zonal-mean net shortwave (Q_{SW}), net longwave (Q_{LW}), sensible (Q_{SE}), and latent (Q_{LT}) heat fluxes are summed up over the inner tropics, a net forcing of 0.1 W m^{-2} (100 sfu)$^{-1}$ warms the ocean surface. The radiation balance calculations of White et al. (1998) estimated that 0.1 W m^{-2} net heating should warm the zonal-mean ocean surface by about 0.03 K. Yet, the simulated SST anomalies in CENS are two to three times stronger in the inner tropics, suggesting that another positive feedback is amplifying the response. This feedback, which operates in the tropical Pacific, is explained in the following section.

b. *Response of ocean dynamics*

To demonstrate the response of the coupled atmosphere–ocean system, regression maps onto F10.7 of the equatorial (5°S–5°N) zonal wind, ocean potential temperature and the vertical gradient of ocean potential temperature are presented (Fig. 10). The latter variable measures the sharpness and the depth of the thermocline (DiNezio et al. 2009).

TABLE 1. Intratropical (10°S–10°N) averages of the surface heat budget over oceans [W m^{-2} (100 sfu)$^{-1}$]. Relative contribution of the clear-sky and cloud forcing is given in the first and second columns. Third column lists the net Q_{SW}, Q_{LW}, Q_{SE}, and Q_{LT} heat flux changes. Positive anomalies point to the ocean.

	Clear sky	Cloud cover	All sky
Q_{SW}	−0.02	+0.19	+0.17
Q_{LW}	+0.3	−0.13	+0.17
Q_{SE}	—	—	+0.03
Q_{LT}	—	—	−0.27
Sum	+0.28	+0.06	+0.1

The zonal wind climatology over the equatorial Pacific (Walker cell) is characterized by easterlies in the lower troposphere and westerlies in the upper troposphere (contours in Fig. 10a). With stronger solar forcing, negative zonal wind anomalies [-0.4 m s^{-1} (100 sfu)$^{-1}$] are simulated at the upper branch of the Walker cell, together with positive anomalies [0.2 m s^{-1} (100 sfu)$^{-1}$] in the lower troposphere. The strongest westerly anomalies are found in the western Pacific just east of the zero wind line and not at the core of the jet, indicating that the western branch of the Walker circulation shifts to the east. Such an eastward movement displaces the region of deep convection, resulting in positive cloud cover and precipitation anomalies over the western Pacific (Figs. 8 and 9c). We note though that the signal is weak and of low significance.

An eastward displacement of the Walker cell causes westerly anomalies at the surface and weakens the zonal wind stress along the western and central parts of the equatorial Pacific, resulting in a number of oceanic changes. For example, a weakening of the equatorial surface currents and equatorial upwelling in concert with a reduced east–west tilt of the thermocline and decreased mean thermocline depth is expected (e.g., Philander 1981). In the following paragraphs, we demonstrate that such changes are simulated in CENS, indeed.

The subsurface warming in the upper layers of the Pacific Ocean reaches values of 0.12 K (100 sfu)$^{-1}$, whereas the sign reverses in the deeper layers (Fig. 10b). The strongest cooling [0.2 K (100 sfu)$^{-1}$] is located in the western Pacific at 160-m depth around the mean thermocline position (dashed black line). A dynamical mechanism causes this cooling. The thermocline shoals in the western Pacific due to the positive wind stress anomalies, while the signal in the east is negligible. In other words, the east–west thermocline tilt is relaxed. At the same time, a basinwide shoaling of the Pacific thermocline is simulated in solar maxima because positive anomalies of the potential temperature gradient flank the 20°C isotherm at shallower layers (Fig. 10c). In the eastern equatorial Indian Ocean, a shallower thermocline is also detected.

A lag-regression analysis of the potential temperature along the equatorial Pacific underlines the importance of thermocline depth changes in controlling the subsurface response (Fig. 11). At lag -5 yr (meaning that F10.7 is leading temperature anomalies by 5 years), positive anomalies at 100–200-m depth are simulated in the western Pacific, which, as time progresses, extend to the east following the mean thermocline depth line and emerge at shallower levels (lag -5 to lag -2). The apparent eastward propagation is attributed to slow equatorial waves, which are coupled to the underlying

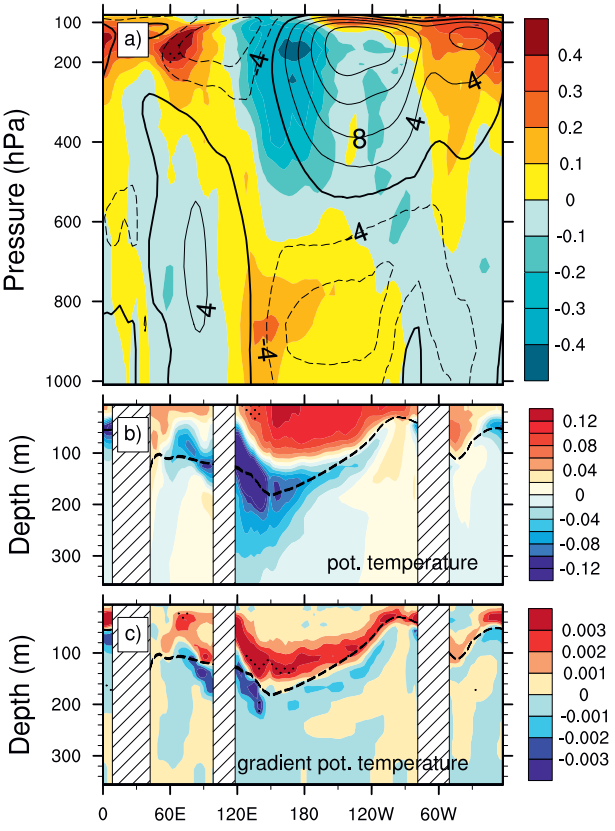

FIG. 10. Regression coefficients (color shading) onto F10.7 of the ensemble-mean annual (a) zonal wind in CENS [m s^{-1} (100 sfu)$^{-1}$], (b) ocean potential temperature [K (100 sfu)$^{-1}$], and (c) gradient of the ocean potential temperature [K m^{-1} (100 sfu)$^{-1}$] along the equator (5°N–5°S). Contours (top panel) show the climatological zonal wind (m s^{-1}) in CTR. Dashed lines (middle and bottom panels) indicate the 20°C isotherm in CTR. Stippled areas indicate 95% significance. The troposphere–lower stratosphere (up to 90 hPa) is shown in (a), while the upper 360 m of the ocean is shown in (b) and (c).

atmosphere, as in the analysis of White et al. (2003). From lag -2 to lag 0, anomalously cold water builds up in place of warm water, completing half a cycle. At lag -1 the subsurface positive anomalies reach the surface and over the next year the warming is amplified.

The origin of this amplification is understood by examining the response of the shallow Pacific overturning circulation. Figure 12 shows the regression coefficients (shading) of the zonal-mean (120°E–70°W) meridional velocity onto F10.7, together with its climatological profile from CTR (contours). With stronger solar activity, a tendency for a slower meridional circulation in the Pacific is simulated, affecting the surface cooling efficiency of the poleward heat transport. In accordance with the slower meridional transport, the upwelling over the entire Pacific basin is reduced, with the strongest

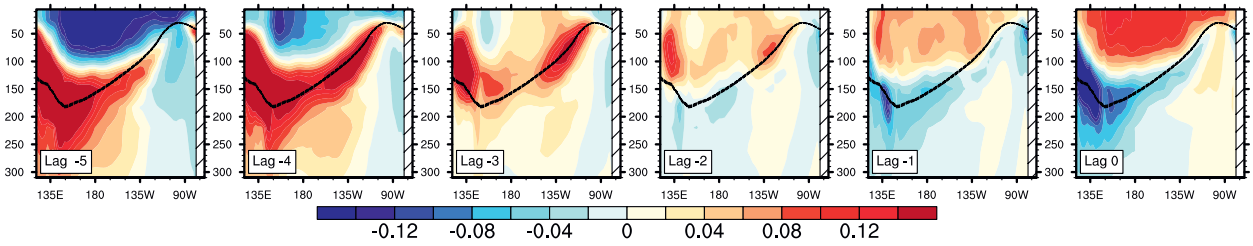

FIG. 11. Time sequences of lagged regression coefficients onto F10.7 of the ensemble-mean annual ocean potential temperature [K (100 sfu)$^{-1}$] along the equator (5°S–5°N). The vertical axis covers the upper 310 m of the ocean. Negative lag (yr) means that F10.7 is leading the ocean potential temperature. No statistical significance is plotted.

signal in the central and western sectors (not shown). As expected, the North Equatorial Counter Current (NECC) weakens with ensuing surface warming due to decreased heat flux divergence (DiNezio et al. 2009).

In the case of warm ENSO events, the thermocline shoals in the western Pacific but deepens in the eastern Pacific. Such an east–west asymmetry is not apparent in CENS. Instead, the thermocline shoals throughout the equatorial Pacific basin with stronger changes in the western part. In the eastern part the thermocline sinking due to reduced surface easterlies is balanced by the zonal average shoaling. These responses to stronger solar forcing resemble the simulated responses of the equatorial Pacific to increased greenhouse gas concentrations [cf. Fig. 10c with Fig. 1a in DiNezio et al. (2010)]. As proposed by DiNezio et al., these two opposing tendencies may yield a condition wherein the eastern Pacific is less prone to surface wind stress anomalies, thus suppressing the efficiency of the Bjerknes feedback (Bjerknes 1966) to amplify weak SST anomalies to El Niño. In CENS, therefore, the El Niño–like signature in the topical Pacific does not reflect a statistical excitation of more El Niño events in solar maxima. Our simulations emphasize the importance of ocean circulation changes induced by reduced surface easterlies. The subsequent reduction of heat transport divergence warms the surface on decadal time scales (Fig. 11). The synergy of ocean circulation changes and the water vapor feedback results in stronger warming over the Pacific Ocean when compared to the solar signals over the Indian and Atlantic Oceans. Further ensemble simulations with MAECHAM5 coupled to a mixed layer ocean (as in Vecchi and Soden 2007) may assess the relative contribution of the dynamic and thermodynamic changes on the tropical Pacific response.

6. Tropical responses to the solar cycle in the uncoupled simulations

The previous section demonstrated the key role of the eastward shift of the region of deep convection. It remains to answer how this shift is physically explained. The ensemble simulations without ocean coupling (AENS) give a plausible answer.

Figure 13 shows the regression coefficients onto F10.7 of the equatorial zonal wind anomalies in AENS and should be compared to Fig. 10a. Although some differences between the AENS and CENS simulations can be seen, particularly in the upper troposphere, the salient feature of Fig. 13 is the eastward displacement of the western branch of the Walker circulation, resulting in weaker surface winds at the equatorial Pacific. This displacement is qualitatively similar to CENS, although the detailed spatial pattern is somewhat different. The latter is likely attributed to the fact that oceanic changes due to reduced surface winds cannot feed back to the atmosphere. In AENS, the signal is statistically robust and stronger compared to CENS. It seems therefore that

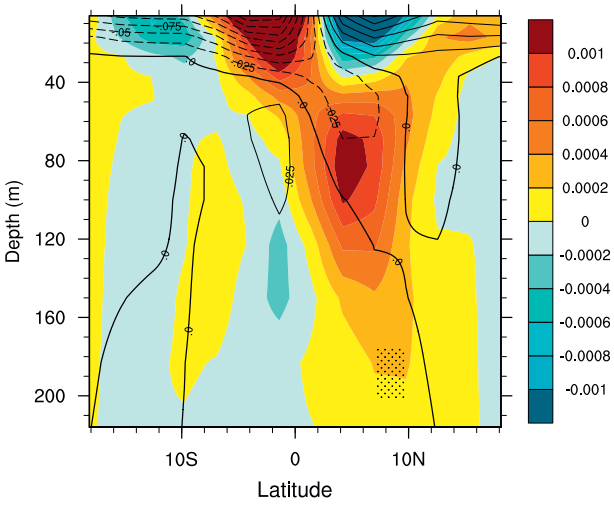

FIG. 12. (shading) Regression coefficients onto F10.7 of the ensemble-mean annual meridional velocity [m s^{-1} (100 sfu)$^{-1}$] averaged over 120°E–70°W. Climatological values from CTR are superimposed (contours) with solid (dashed) lines to denote positive (negative) values (contour interval: 0.025 m s^{-1}).The vertical axis covers the upper 220 m of the ocean. Stippling indicates 95% significance.

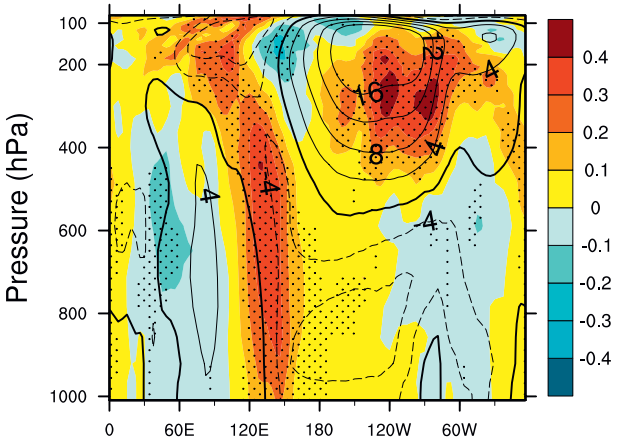

FIG. 13. Regression coefficients onto F10.7 of the ensemble-mean annual zonal wind anomalies (color shading) along the equator in AENS [m s^{-1} (100 sfu)$^{-1}$]. Contours show the zonal wind (m s^{-1}) climatology in CTR. Stippling indicates 95% significance. Compare to Fig. 10a.

ocean coupling is not needed to simulate an eastward shift of the Walker circulation. In fact, increased stratification in the eastern Pacific in solar maxima could act to weaken the atmospheric response in solar maxima (Clement et al. 1996). Simulations of the atmospheric and oceanic response to increasing greenhouse gas concentrations led to a similar conclusion (Vecchi and Soden 2007; DiNezio et al. 2009).

In AENS, the deep convection in the western Pacific moves to the west following the changes in the Walker circulation. This displacement takes the form of a negative/positive dipole between 100° and 150°E in the total precipitation anomalies (shading in Fig. 14). Furthermore, the precipitation over the ITCZ strengthens. Indicated in Fig. 13 already, the surface easterlies slow down in the tropical Pacific and the strongest wind stress changes are simulated in the western sector (vectors in Fig. 14). Given that quantitatively and qualitatively similar responses are simulated in CENS, we conclude that the atmospheric response to the solar cycle is driving the tropical Pacific response.

It is difficult to trace the origin of these atmospheric changes with the current set of experiments. Nevertheless, the suggestion of Held and Soden (2006) provides a plausible explanation. They suggested that under global warming, the zonally asymmetric component of the atmospheric overturning circulation should slow down in response to differential changes of global-mean precipitation and low-tropospheric water vapor. Simulations of global warming caused by increased greenhouse gas concentrations show a 2% K^{-1} increase of global-mean precipitation opposed to a 7% K^{-1} increase of low-tropospheric water vapor (Vecchi and Soden 2007). To balance this difference, the atmospheric overturning circulation—and particularly the Walker circulation—is weakening and at the same time deep convection shifts to the east (Held and Soden 2006; Vecchi and Soden 2007).

A globally warmer climate is also anticipated with increased solar activity (e.g., Gray et al. 2010). The CENS simulations exhibit an increase of 0.034 K (100 sfu)$^{-1}$ in global-mean 2-m temperature, 0.352% (100 sfu)$^{-1}$ in global-mean vertically integrated water vapor, and 0.048% (100 sfu)$^{-1}$ in global-mean total precipitation. These numbers translate to approximately a 10% K^{-1} increase of the rate of low-tropospheric water vapor (the vertically integrated water vapor reflects humidity changes in the boundary layer) and a 1.4% K^{-1} increase in total precipitation. Hence, in our simulations the sensitivity of the rate of moistening and precipitation to increased solar forcing is consistent with the simulated response to increased greenhouse gas concentrations. Changes in the atmospheric hydrology, therefore, may explain the displacement of the Walker circulation, which in turn leads to westerly anomalies and warming over the tropical Pacific Ocean. It must be noted that the previous derivations cannot be repeated for AENS because of the prescribed surface boundary.

7. Potential model shortcomings

Although the amplitude of the positive SST anomalies in the Pacific as simulated with MAECHAM5/MPI-OM is consistent with solar cycle signals in observations (White et al. 1997), the globally averaged temperature response is substantially weaker. Our model shows a global (60°S–60°N) ocean surface warming on the order of 0.027 K (100 sfu)$^{-1}$ or 0.036 K from solar minimum to maximum (average difference of 133 sfu). This number is roughly half of the observed global ocean temperature response (0.08 K) to 11-yr solar forcing (White et al. 1997; Tung and Camp 2008). If temperature changes over land surface are added, the simulated global-mean warming is slightly stronger [0.03 K (100 sfu)$^{-1}$ or 0.04 K for solar maximum–solar minimum]. Yet, the signal remains considerably lower than the observed 0.1 K warming from minimum to maximum phase of solar activity (Lean and Rind 2008).

It is particularly challenging to understand why our simulations underestimate the global response while they give a reasonable signal over the tropical Pacific when compared to the work of White et al. (1997). One reason could be deficiencies in simulating a realistic reduction of the global planetary albedo due to cloud changes. One of the major caveats of current AOGCMs are uncertainties related to the parameterization of

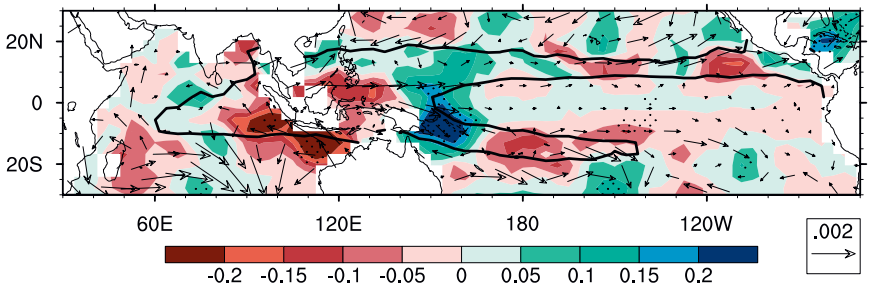

FIG. 14. Regression coefficients onto F10.7 of the ensemble-mean annual total precipitation [mm day^{-1} (100 sfu)$^{-1}$] (shading) and wind stress anomalies [N m^{-2} (100 sfu)$^{-1}$] (vectors in AENS). Stippling indicates 95% significance of the total precipitation changes. The thick black line outlines areas where the total precipitation climatology in CTR exceeds 6 mm day^{-1}. Compare to Fig. 8.

clouds. For example, the proper simulation of marine stratocumulus clouds in the eastern Pacific is still a major issue (Lin 2007).

One important shortcoming of our model is the poor representation of the solar cycle effects in the Northern Hemisphere (NH) winter stratosphere. The simulated polar vortex stays anomalously weak during solar maxima, resulting in negative zonal wind anomalies throughout the winter. This response is not consistent with earlier analyses of observations and simulations (Kodera and Kuroda 2002; Matthes et al. 2004; Schmidt et al. 2010) and is likely explained by weak heating rate changes to solar forcing in the upper stratosphere when compared to the heating rates calculated with HAMMONIA (Schmidt et al. 2010). This discrepancy results from the coarse spectral resolution of the MAECHAM5 radiation scheme (two spectral bands between 185 and 440 nm). When the solar cycle heating in the stratosphere is deliberately amplified to match HAMMONIA heating rates, the simulated solar cycle signals in the NH stratosphere are closer to those observed.

Probably related to the poor model performance in the NH stratosphere, the ensemble-mean annual temperature response to the solar cycle does not take the form of two separate maxima in the tropical stratosphere. A single temperature maximum in the upper tropical stratosphere (~2 hPa) of about 0.5 K (100 sfu)$^{-1}$ is simulated, instead. In contrast, analyses of observations detected two distinct temperature response maxima in the upper and lower tropical stratosphere, although the origin of the second one is still debated (Gray et al. 2010). Given that the top-down propagation of the solar signals from the stratosphere to the troposphere may amplify the ocean–atmosphere responses to increased TSI (van Loon et al. 2007), this caveat could locally weaken the surface response in our simulations. However, the global-mean signal should remain unaffected.

The simulated solar cycle signals documented in the previous sections are generally weak and insignificant. This does not mean that stronger signals are expected per se, but it suggests that 11 ensemble members that cover five solar cycles are not sufficient for detecting robust responses. Depending on the simulated ENSO amplitude, more than 11 ensemble members or longer simulations may be needed.

8. Conclusions

The goal of this work is to better understand the response of tropical oceans to the 11-yr solar cycle forcing. The focus is on the Pacific Ocean where coupled atmosphere–ocean interactions may amplify solar cycle signals in a way that they resemble El Niño or La Niña. To address this possibility, we analyze an ensemble of 11 simulations (CENS) carried out with MAECHAM5/MPI-OM. Simulations with an atmosphere-only version of the model (AENS) are additionally considered. Both configurations are solely forced with realistic spectral irradiance and ozone changes over the period 1955–2006. This approach diminishes the risk of any solar signal aliasing by other external forcings (e.g., volcanoes, greenhouse gases).

Our analysis is primarily based on unfiltered data; yet bandpass filtering with multichannel singular spectrum analysis (MSSA) is used complementarily to eliminate the strong ENSO signature in the central and eastern Pacific. In the western Pacific, solar-cycle-related changes are detected even in the unfiltered ensemble-mean time series. If increased solar forcing triggers, statistically, more La Niña events and the tropical Pacific shifts to an El Niño state a few years later, as suggested by Meehl and Arblaster (2009), then this cold-to-warm transition is ''smeared out'' when filtering is applied. Our simulations, however, do not support this transition, given that

the warming over the Pacific in CENS is independent of the filtering (Fig. 7). Furthermore, the time evolution of the subsurface temperature anomalies along the equator gives no sign of such a rapid transition (Fig. 11). Instead, it takes almost five years to complete a warm-to-cold transition.

White and Liu (2008a) suggested a nonlinear mechanism by which La Niña–El Niño pairs are aligned to the observed tropical Pacific quasi-decadal oscillation (TPQDO). In particular, they argued that these alignments arise from nonlinear phase locking of third and fifth harmonics (3.6- and 2.2-yr ENSO frequencies) to the first harmonic near the 11-yr period. The first harmonic, which refers to the TPQDO, was excited only in solar-cycle-forced simulations, whereas it was absent when the solar forcing remained constant. This fact implies that the TPQDO is excited by the 11-yr solar cycle. MAECHAM5/MPI-OM as well as other atmosphere–ocean general circulation models, however, simulates a TPQDO even in the control run where the solar forcing is constant. The observed TPQDO, therefore, could be a naturally excited mode of the tropical Pacific. If this is correct, the nonlinear cascade of harmonics suggested by White and Liu (2008a) could be explained without invoking the 11-yr solar cycle and consequently, the transition from La Niña to El Niño in observations could be unrelated to the solar cycle.

The tropical oceans in CENS warm in solar maxima, and the warming is amplified over the Pacific. There, an almost basinwide warming of 0.1 K $(100\ \text{sfu})^{-1}$ is simulated (0.13 K from solar minimum to solar maximum). Both regression analysis and MSSA agree reasonably well on the spatial patterns of the surface warming. In the subsurface western Pacific, however, negative temperature anomalies are simulated. This implies that dynamical changes may penetrate the solar signal deeper than previously thought (White et al. 1997).

The simulated tropical response to solar forcing is pinned down to the synergetic effect of water vapor feedback, cloud changes, and, most importantly, ocean dynamics. As the incoming solar radiation increases, the oceans evaporate more water into the atmosphere. The stronger net downward longwave and shortwave radiation due to increased humidity and reduced cloud cover are sources for surface heating in the Indian and Pacific Oceans, respectively. Hence, the suggestion of Meehl et al. (2008) concerning the contribution of water vapor is confirmed by our simulations. Nevertheless, changes of the surface heat budget cannot explain the magnitude of the surface warming in the tropical Pacific. The stronger tropical Pacific warming is primarily administered by the oceanic responses to reduced surface easterlies, which result from the eastward displacement of the Walker circulation. Such a displacement, including an eastward shift of deep convection, is simulated independently of ocean coupling.

The reduced surface easterlies over the tropical Pacific lift the mean depth of the thermocline and relax its east–west tilt. Additionally, the surface ocean currents and the shallow meridional circulation slacken. These changes weaken the oceanic heat transport, which together with the water vapor feedback amplifies the surface warming. Although the spatial characteristics of the simulated tropical Pacific warming are characterized as El Niño like, the subsurface response shows no evidence for a statistical excitation of more El Niño episodes in solar maxima. This is consistent with the tropical Pacific response to global warming due to increased greenhouse gas concentrations (Vecchi and Soden 2007; DiNezio et al. 2010).

To summarize, the tropical Pacific in our model does not shift to a La Niña–like state in years of peak solar activity, but rather a basinwide warming of about 0.1 K is simulated. It is found that the atmospheric response to the 11-yr solar cycle drives the tropical Pacific response, which is amplified by typical climate feedbacks operating on decadal time scales. Based on our simulations, we expect a warmer tropical Pacific when the sun is more active.

Acknowledgments. We thank Daniela Matei, Gabriel Chiodo, Eleni Vagena, and two reviewers for useful comments on the original manuscript. We also thank the Deutsches Klimarechenzentrum (DKRZ) for providing computational support. This study was funded by the Deutsche Forschungsgemeinschaft (DFG) with the ARTOS project and is part of the doctoral thesis of S. Misios.

REFERENCES

Bal, S., S. Schimanke, T. Spangehl, and U. Cubasch, 2011: On the robustness of the solar cycle signal in the Pacific region. *Geophys. Res. Lett.,* **38,** L14809, doi:10.1029/2011GL047964.

Bjerknes, J., 1966: A possible response of the atmospheric Hadley circulation to equatorial anomalies of ocean temperature. *Tellus,* **18,** 820–829.

Cagnazzo, C., E. Manzini, M. A. Giorgetta, P. M. D. Forster, and J. J. Morcrette, 2007: Impact of an improved shortwave radiation scheme in the MAECHAM5 general circulation model. *Atmos. Chem. Phys.,* **7,** 2503–2515.

Camp, C. D., and K.-K. Tung, 2007: Surface warming by the solar cycle as revealed by the composite mean difference projection. *Geophys. Res. Lett.,* **34,** L14703, doi:10.1029/2007GL030207.

Christoforou, P., and S. Hameed, 1997: Solar cycle and the Pacific 'centers of action.' *Geophys. Res. Lett.,* **24,** 293–296.

Cibot, C., E. Maisonnave, L. Terray, and B. Dewitte, 2005: Mechanisms of tropical Pacific interannual-to-decadal variability in

the ARPEGE/ORCA global coupled model. *Climate Dyn.,* **24,** 823–842.

Clement, A. C., R. Seager, M. A. Cane, and S. E. Zebiak, 1996: An ocean dynamical thermostat. *J. Climate,* **9,** 2190–2196.

Deser, C., M. A. Alexander, S. P. Xie, and A. S. Phillips, 2010: Sea surface temperature variability: Patterns and mechanisms. *Annu. Rev. Mar. Sci.,* **2,** 115–143.

DiNezio, P. N., A. C. Clement, G. A. Vecchi, B. J. Soden, and B. P. Kirtman, 2009: Climate response of the equatorial Pacific to global warming. *J. Climate,* **22,** 4873–4892.

——, ——, and ——, 2010: Reconciling differing views of tropical Pacific climate change. *Eos, Trans. Amer. Geophys. Union,* **91,** 141, doi:10.1029/2010EO160001.

Eyring, V., T. G. Shepherd, and W. D. Waugh, Eds., 2010: SPARC report on the evaluation of Chemistry-Climate Models. SPARC Rep. 5, WCRP-132, WMO/TD-1526, 434 pp.

Ghil, M., and Coauthors, 2002: Advanced spectral methods for climatic time series. *Rev. Geophys.,* **40,** 1003, doi:10.1029/2000RG000092.

Gray, L. J., and Coauthors, 2010: Solar influences on climate. *Rev. Geophys.,* **48,** RG4001, doi:10.1029/2009RG000282.

Guilyardi, E., P. Delecluse, S. Gualdi, and A. Navarra, 2003: Mechanisms for ENSO phase change in a coupled GCM. *J. Climate,* **16,** 1141–1158.

Hasegawa, T., and K. Hanawa, 2003: Decadal-scale variability of upper ocean heat content in the tropical Pacific. *Geophys. Res. Lett.,* **30,** 1272, doi:10.1029/2002GL016843.

Held, I. M., and B. J. Soden, 2006: Robust responses of the hydrological cycle to global warming. *J. Climate,* **19,** 5686–5699.

Jin, F. F., 1997: An equatorial ocean recharge paradigm for ENSO. Part I: Conceptual model. *J. Atmos. Sci.,* **54,** 811–829.

Jungclaus, J. H., and Coauthors, 2006: Ocean circulation and tropical variability in the coupled model ECHAM5/MPI-OM. *J. Climate,* **19,** 3952–3972.

Klein, S. A., and D. L. Hartmann, 1993: The seasonal cycle of low stratiform clouds. *J. Climate,* **6,** 1587–1606.

Knutson, T. R., and S. Manabe, 1998: Model assessment of decadal variability and trends in the tropical Pacific Ocean. *J. Climate,* **11,** 2273–2296.

Kodera, K., and Y. Kuroda, 2002: Dynamical response to the solar cycle. *J. Geophys. Res.,* **107,** 4749, doi:10.1029/2002JD002224.

Lean, J. L., and D. H. Rind, 2008: How natural and anthropogenic influences alter global and regional surface temperatures: 1889 to 2006. *Geophys. Res. Lett.,* **35,** L18701, doi:10.1029/2008GL034864.

Lee, J. N., D. T. Shindell, and S. Hameed, 2009: The influence of solar forcing on tropical circulation. *J. Climate,* **22,** 5870–5885.

Lin, J.-L., 2007: The double-ITCZ problem in IPCC AR4 coupled GCMs: Ocean–atmosphere feedback analysis. *J. Climate,* **20,** 4497–4525.

Manzini, E., M. A. Giorgetta, M. Esch, L. Kornblueh, and E. Roeckner, 2006: The influence of sea surface temperatures on the northern winter stratosphere: Ensemble simulations with the MAECHAM5 model. *J. Climate,* **19,** 3863–3881.

Marsland, S. J., H. Haak, J. H. Jungclaus, M. Latif, and F. Röske, 2003: The Max-Planck-Institute global ocean/sea ice model with orthogonal curvilinear coordinates. *Ocean Modell.,* **5,** 91–127.

Matthes, K., U. Langematz, L. L. Gray, K. Kodera, and K. Labitzke, 2004: Improved 11-year solar signal in the Freie Universität Berlin Climate Middle Atmosphere Model (FUB-CMAM). *J. Geophys. Res.,* **109,** D06101, doi:10.1029/2003JD004012.

——, Y. Kuroda, K. Kodera, and U. Langematz, 2006: Transfer of the solar signal from the stratosphere to the troposphere: Northern winter. *J. Geophys. Res.,* **111,** D06108, doi:10.1029/2005JD006283.

Meehl, G. A., and J. M. Arblaster, 2009: A lagged warm event–like response to peaks in solar forcing in the Pacific region. *J. Climate,* **22,** 3647–3660.

——, W. M. Washington, T. M. L. Wigley, J. M. Arblaster, and A. Dai, 2003: Solar and greenhouse gas forcing and climate response in the twentieth century. *J. Climate,* **16,** 426–444.

——, J. M. Arblaster, G. Branstator, and H. van Loon, 2008: A coupled air–sea response mechanism to solar forcing in the Pacific region. *J. Climate,* **21,** 2883–2897.

——, ——, K. Matthes, F. Sassi, and H. van Loon, 2009: Amplifying the Pacific climate system response to a small 11-year solar cycle forcing. *Science,* **325,** 1114–1118.

Meinen, C. S., and M. J. McPhaden, 2000: Observations of warm water volume changes in the equatorial Pacific and their relationship to El Niño and La Niña. *J. Climate,* **13,** 3551–3559.

Philander, S. G. H., 1981: The response of equatorial oceans to a relaxation of the trade winds. *J. Phys. Oceanogr.,* **11,** 176–189.

Plaut, G., and R. Vautard, 1994: Spells of low-frequency oscillations and weather regimes in the Northern Hemisphere. *J. Atmos. Sci.,* **51,** 210–236.

Reichler, T., and J. Kim, 2008: How well do coupled models simulate today's climate? *Bull. Amer. Meteor. Soc.,* **89,** 303–311.

Rind, D., J. Lean, J. Lerner, P. Lonergan, and A. Leboissitier, 2008: Exploring the stratospheric/tropospheric response to solar forcing. *J. Geophys. Res.,* **113,** D24103, doi:10.1029/2008JD010114.

Roeckner, E., and Coauthors, 2006: Sensitivity of simulated climate to horizontal and vertical resolution in the ECHAM5 atmosphere model. *J. Climate,* **19,** 3771–3791.

Roy, I., and J. D. Haigh, 2010: Solar cycle signals in sea level pressure and sea surface temperature. *Atmos. Chem. Phys.,* **10,** 3147–3153.

Schmidt, H., G. P. Brasseur, and M. A. Giorgetta, 2010: Solar cycle signal in a general circulation and chemistry model with internally generated quasi-biennial oscillation. *J. Geophys. Res.,* **115,** D00I14, doi:10.1029/2009JD012542.

Shindell, D. T., G. Faluvegi, R. L. Miller, G. A. Schmidt, J. E. Hansen, and S. Sun, 2006: Solar and anthropogenic forcing of tropical hydrology. *Geophys. Res. Lett.,* **33,** L24706, doi:10.1029/2006GL027468.

Smith, T. M., R. W. Reynolds, T. C. Peterson, and J. Lawrimore, 2008: Improvements to NOAA's historical merged land–ocean surface temperature analysis (1880–2006). *J. Climate,* **21,** 2283–2296.

Thompson, D. W. J., J. J. Kennedy, J. M. Wallace, and P. D. Jones, 2008: A large discontinuity in the mid-twentieth century in observed global-mean surface temperature. *Nature,* **453,** 646–649.

Tourre, Y. M., C. Cibot, L. Terray, W. B. White, and B. Dewitte, 2005: Quasi-decadal and inter-decadal climate fluctuations in the Pacific Ocean from a CGCM. *Geophys. Res. Lett.,* **32,** L07710, doi:10.1029/2004gl022087.

Tung, K.-K., and C. D. Camp, 2008: Solar cycle warming at the earth's surface in NCEP and ERA-40 data: A linear discriminant analysis. *J. Geophys. Res.,* **113,** D05114, doi:10.1029/2007JD009164.

——, and J. Zhou, 2010: The Pacific's response to surface heating in 130 yr of SST: La Niña–like or El Niño–like? *J. Atmos. Sci.,* **67,** 2649–2657.

Valcke, S., D. Caubel, D. Declat, and L. Terray, Eds., 2003: OASIS3: Ocean atmosphere sea ice soil user's guide. PRISM Project Rep. 2, CERFACS TR/CMGC/03/69, 57 pp.

van Loon, H., and G. A. Meehl, 2011: The average influence of decadal solar forcing on the atmosphere in the South Pacific region. *Geophys. Res. Lett.,* **38,** L12804, doi:10.1029/2011GL047794.

——, ——, and J. M. Arblaster, 2004: A decadal solar effect in the tropics in July–August. *J. Atmos. Sol. Terr. Phys.,* **66,** 1767–1778.

——, ——, and D. J. Shea, 2007: Coupled air-sea response to solar forcing in the Pacific region during northern winter. *J. Geophys. Res.,* **112,** D02108, doi:10.1029/2006JD007378.

Vecchi, G. A., and B. J. Soden, 2007: Global warming and the weakening of the tropical circulation. *J. Climate,* **20,** 4316–4340.

White, W. B., and Z. Liu, 2008a: Non-linear alignment of El Niño to the 11-yr solar cycle. *Geophys. Res. Lett.,* **35,** L19607, doi:10.1029/2008GL034831.

——, and ——, 2008b: Resonant excitation of the quasi-decadal oscillation by the 11-year signal in the sun's irradiance. *J. Geophys. Res.,* **113,** C01002, doi:10.1029/2006JC004057.

——, J. Lean, D. R. Cayan, and M. D. Dettinger, 1997: Response of global upper ocean temperature to changing solar irradiance. *J. Geophys. Res.,* **102** (C2), 3255–3266.

——, D. R. Cayan, and J. Lean, 1998: Global upper ocean heat storage response to radiative forcing from changing solar irradiance and increasing greenhouse gas/aerosol concentrations. *J. Geophys. Res.,* **103** (C10), 21 355–21 366.

——, Y. M. Tourre, M. Barlow, and M. Dettinger, 2003: A delayed action oscillator shared by biennial, interannual, and decadal signals in the Pacific basin. *J. Geophys. Res.,* **108,** 3070, doi:10.1029/2002JC001490.

Wilks, D. S., 2006: *Statistical Methods in the Atmospheric Sciences*. 2nd ed. International Geophysics Series, Vol. 91, Academic Press, 627 pp.

Zhou, J. S., and K.-K. Tung, 2010: Solar cycles in 150 years of global sea surface temperature data. *J. Climate,* **23,** 3234–3248.